View metadata, citation and similar papers at core.ac.uk

brought to you by CORE

provided by RMIT Research Repository

Thank you for downloading this document from the RMIT Research Repository.

The RMIT Research Repository is an open access database showcasing the research outputs of RMIT University researchers.

RMIT Research Repository: http://researchbank.rmit.edu.au/

Citation:

Donough, M, Gunnion, A, Orifici, A and Wang, C 2015, 'Scaling parameter for fatigue delamination growth in composites under varying load ratios', Composites Science and Technology, vol. 120, pp. 39-48.

See this record in the RMIT Research Repository at:

https://researchbank.rmit.edu.au/view/rmit:34176

Version: Accepted Manuscript

Copyright Statement: © 2015 Elsevier Ltd. Creative Commons Attribution-NonCommercial-NoDerivatives 4.0 International License.

Link to Published Version:

http://dx.doi.org/10.1016/j.compscitech.2015.10.011

PLEASE DO NOT REMOVE THIS PAGE

Scaling Parameter for Fatigue Delamination Growth in Composites under Varying Load Ratios

M.J. Donough[1,2], A.J. Gunnion[2,3], A.C. Orifici[1] and C.H. Wang[1]□*

[1] *Sir Lawrence Wackett Aerospace Research Centre, School of Aerospace, Mechanical and Manufacturing Engineering, RMIT University, GPO Box 2476, Melbourne, Victoria 3001, Australia*
[2] *CRC-ACS, 1/320 Lorimer Street, Port Melbourne, Victoria 3207, Australia*
[3] *ACS Australia, 1/320 Lorimer Street, Port Melbourne, Victoria 3207, Australia*

Keywords: A. Polymer-matrix composites (PMCs), Delamination, C. Fibre bridging

Abstract

Fatigue delamination growth in composite laminates is strongly influenced by mean loads or load ratios. Description of this behaviour currently relies on empirical curve fitting, which renders it difficult to predict fatigue lives of composite structures subjected to variable amplitude fatigue loading. This paper presents a new scaling parameter that is consistent with the similitude concept and incorporates the crack-tip shielding effects of fibre bridging under fatigue loading. Static and fatigue experiments were carried out on IM7/977-3 composite laminates under mode I and mode II. Large scale fibre bridging was observed as a major toughening mechanism under both static and fatigue loading. To correctly account for the effect of fibre bridging, an inverse method was developed to determine the traction stresses acting in the crack wake. The new scaling parameter, accounting for the fatigue bridging traction, is shown to unify the fatigue growth rates under different load ratios obtained in this study.

1. Introduction

In aerospace applications, composite structures must be designed for no-growth or slow fatigue crack growth, according to the current airworthiness regulations [1], to prevent manufacturing defects or in-service damage (e.g. resulting from low energy impact) from reaching the safety limits. Traditionally, this is typically accomplished by employing low design allowable strains, validated by fatigue tests demonstrating that defects of the minimum detection size do not grow under service loading. Although slow-growth (near threshold region) mode is permitted in

□* Correspondence author: C. H. Wang *Tel: +61 3 99256115, e-mail: chun.wang@rmit.edu.au*

demonstrating compliance with airworthiness regulations, the no-growth criterion is more commonly used, due to the lack of a better design criterion for slow fatigue crack growth of composites under fatigue loading. Delamination crack has been observed to propagate under fatigue loading far below the static fracture loads [2]. As a result, existing composite structure designs using the no-growth criterion often carry additional weight to mitigate the risk of fatigue failure from service-induced damage. To fully take advantages of the lightweight characteristics of composite materials and to reduce the high cost burden of existing design practices, it is important to quantify the near-threshold growth behaviour to ensure the continuous airworthiness of composite structures during service [1] without excessive component and full-scale testing.

In contrast to metallic alloys, fibre-reinforced composites are highly anisotropic and inhomogeneous. The strain energy release rate (G), rather than the stress intensity factor (K), is commonly used to correlate the fatigue delamination growth rates. This is because the solution for K is highly complex for inhomogeneous materials and can result in oscillatory stresses between plies of different elastic properties [3]. The delamination growth of composite laminates is conventionally described in terms of the strain energy release rate G by a Paris-law type of relation given below, with C and exponent m being fitting parameters that depend on materials and load ratios,

$$\frac{da}{dN} = C\left(\Delta G\right)^m \tag{1}$$

where the cyclic strain energy release rate ΔG is defined as the difference between the applied maximum and minimum values [4-7],

$$\Delta G = G_{\max}^{app} - G_{\min}^{app} \tag{2}$$

One major drawback of the above ΔG definition is that it does not conform to the similitude principle (i.e. crack-tip conditions are uniquely defined by a single loading parameter) similar to ΔK [8-10]. Moreover there is a potential ambiguity in this definition for negative load ratios ($R = P_{\min} / P_{\max} < 0$). For example, ΔG equals zero under fully reversed loading ($R = -1$), because the G_{max} and G_{min} are equal. In addition, strong load ratio effects have been observed for both mode I and II fatigue behaviour when ΔG is employed as the correlating parameter [9, 11]. Consequently the coefficients C and m in Eq. (1) must be empirically determined for a given specific load ratio [4].

To avoid the ambiguity associated with ΔG, the maximum strain energy release rate $G_{\max}^{app}$ has been used as the correlating linear elastic fracture mechanics parameter. However $G_{\max}^{app}$ inherently cannot account for the influence of load ratios. Hence Andersons *et al*. developed a model based on linear damage accumulation to predict the effects of load ratios on mode I and II delamination fatigue behaviour [12]. While reasonably good correlation can be obtained, the model requires a

number of additional parameters which must be calibrated or determined experimentally. Allegri *et al*. proposed a two-parameter fatigue delamination model for mode II loading [13], which was later extended to account for both load ratios and mixed mode ratios [14]. Jones and colleagues proposed a modified Hartman-Schijve relation for composite delamination [15] and bonded joints [16], in which the threshold and toughness values are calibrated experimentally for varying load ratios.

Given the lack of physical basis of the ΔG definition, an alternative definition for an equivalent strain energy release rate has recently been suggested [8-10, 17, 18] for correlating delamination growth and disbond growth in joints,

$$\Delta G_{eq} = \left(\sqrt{G_{\max}^{app}} - \sqrt{G_{\min}^{app}} \right)^2 = (1-R)^2 G_{\max}^{app} \tag{3}$$

The equivalent strain energy release rate ΔG_{eq} parameter assumes that delamination growth is controlled by the cyclic stress state at the crack tip, consistent with the similitude principle as ΔK for fully open fatigue cracks in metallic alloys [19]. When experimental delamination growth rate data are expressed in terms of ΔG_{eq}, the strong load ratios effects are nevertheless observed in the mode I fatigue behaviour [8-10, 17, 18]. Therefore empirical fitting parameters are still needed to correlate data pertinent to different load ratios.

In addition to the need for extensive experimental tests to determine the necessary fitting parameters, the aforementioned empirical approaches are difficult to model the transient effect of overloads and underloads under variable amplitude loading, which is essential to the estimation of fatigue life under spectrum loading. Motivated by the great success of the crack closure concept in quantifying the effects of variable amplitude loading on the fatigue crack growth in metallic alloys [20-22], the present authors have recently shown that the load ratio effects on the disbond growth in bonded joints can be characterised by an effective strain energy release rate, once the plasticity-induced crack closure has been taken into account [10]. By contrast to metallic alloys and adhesives, fibre-reinforced composites are known to exhibit extrinsic toughening by fibre bridging [18, 23-26]. The aim of this paper is to extend the effective strain energy concept to quantify the effects of fibre bridging on the fatigue delamination behaviour of composite laminates. Double cantilever beam (DCB) and end-notched flexure (ENF) specimens were manufactured from unidirectional carbon-epoxy composite laminates. Static and fatigue tests were carried out during which the fibre bridging traction stresses were quantified. Then an inverse method was developed with the aid of finite element (FE) analyses to quantify the effects of fibre bridging on the strain energy release rate at the crack tip. Based on these results, a new scaling parameter is proposed which is shown to correlate well with both mode I and II fatigue delamination growth rates.

2. Materials and Methodology

2.1. Materials and Specimen Preparation

Composite laminates were fabricated from 24-ply unidirectional IM7/977-3 pre-pregs with a nominal ply thickness of 0.13 mm. A starter delamination was introduced in the mid-plane by inserting a 13 µm thick poly-tetrafluoroethylene (PTFE) film. The composite laminates were cured in an autoclave at 177 °C under a pressure of 538 kPa for 6 h in accordance to the manufacturer's recommended cure cycle. The test specimens were then machined from the laminates with a diamond saw into the following dimensions; 20 mm width, 170 mm length and a starter crack of a_0 = 70 mm. Additional piano hinges were glued to the DCB specimens with a two-component epoxy. The side of the specimens were painted with a thin coat of white, brittle correction fluid to aid visual observation of the crack.

2.2. Static Test Procedure

Mode I and II fracture toughness tests were performed with DCB and ENF specimens respectively using Instron 4466 with a 10 kN load cell. A schematic of the test configuration is shown in Fig.1. The initial crack position of the ENF specimen was placed at $a_0 = 0.5L$ to provide sufficient length for delamination growth. Specimens were loaded under displacement control at a rate of 0.1 mm/min. The delamination length was measured visually from the travelling microscope. The mode I and II fracture energies, G_I and G_{II}, were then calculated using the beam theory method and are expressed in Eq. (4) and (5) respectively [27-29].

$$G_I = \frac{3P\Delta_{applied}}{2Ba} \tag{4}$$

$$G_{II} = \frac{9a^2 P\Delta_{applied}}{2B\left(2L^3 + 3a^3\right)} \tag{5}$$

where a is the crack length, B is the specimen width, P is the reaction force, Δ is the applied crosshead displacement and L is the span of the support rollers in the ENF test configuration.

2.3. Fatigue Test Procedure

Fatigue experiments were conducted on a computer-controlled all-electric Instron E3000 system with a 3 kN load cell. The specimens were subjected to constant amplitude, sinusoidal cyclic load with a frequency of 10 Hz under displacement control. A sharp delamination front was introduced from the PTFE pre-cracks under relatively high cyclic loads prior to the start of the experiment. The maximum applied load for the tests was chosen to be approximately 50-60% of the maximum fracture energy G_{IR}, determined from the monotonic tests. After an initial 100-1000 cycles

when delamination growth was visible, the delamination lengths were then recorded, from which growth rates were calculated. The fatigue delamination growth rates in the Paris plot were generated using the load-shedding scheme prescribed in ASTM E647 [30]. Mode I tests were conducted at load ratios R of 0.1, 0.3 and 0.5, while mode II tests were conducted at load ratios of 0 and 0.45. In order to account for the cyclic loads, the cyclic strain energy release rate is defined as ΔG_{eq}, given in Eq. (3). This definition was selected to characterise the delamination growth rates because it maintains the theoretical requirement of similitude under fatigue. G_{max} and G_{min} can be calculated from the respective reaction loads at maximum and minimum applied displacements using the beam theory method, shown in Eq. (4) and (5) for mode I and II.

In order to further investigate the effect of fibre bridging on the fatigue delamination growth rates, another set of tests were carried out using DCB specimens under a constant maximum strain energy release rates $G_{\max}^{app}$ of 150 J/m^2 (63% of critical resistance energy $G_{IRC,}$ referring to Section 3.1), R = 0.1 and 0.3. To keep the maximum strain energy release rate approximately constant, the tests were interrupted after 0.5 mm delamination growth. The applied displacement was recalculated and adjusted to maintain $G_{\max}^{app}$ corresponding to the new delamination length. During the tests, the delamination lengths were recorded and used for determining the growth rates.

3. Experimental Results and Discussion

3.1. Static Fracture

Stick-slip crack growth behaviour was observed for the DCB specimen. The mode I delamination growth resistance (R) curve which is the relation of the energy (G_{IR}) needed to advance the crack tip and the delamination length extension (Δa), is shown in Fig. 2. The initial value of mode I fracture toughness, G_{IR0} (at Δa = 0 mm), was measured at 100 J/m^2. As the delamination propagated, G_{IR} gradually increases and becomes independent of crack length increment after a characteristic propagation distance of Δa = 23 mm. The averaged value of the steady-state fracture resistance, denoted as G_{IRC}, is 240 J/m^2, representing an increase of 140% from the initial value. The significant increase of the mode I fracture resistance can be attributed to the bridging by cross-over fibres behind the crack tip, which was observed in the present study and commonly reported in the literature [18, 24-26, 31, 32]. In mode II tests, no R-curve has been observed (hence the results are not shown) and the average value of the mode II critical fracture energy is 1000 J/m^2.

Under static fracture condition, the traction stress [23, 24, 33] as a function of the crack opening displacement, $\sigma_{sb} = \sigma_{sb}(\delta)$, is position independent, i.e., the same for every point in the bridging

zone. The traction stress would decrease monotonically from a maximum σ_{br} at the crack tip to zero towards the end of the bridging zone at maximum separation. From the J-integral conservation, the energy for an advancing crack can then be summarised as

$$G_{IR} = G_{IRC0} + G_{sb} = G_{IRC0} + \int_0^{\delta_{a0}} \sigma_{sb}(\delta) d\delta \tag{6}$$

where δ_{a0} represents the separation at the pre-crack tip location. G_{IRC0} is the matrix material's intrinsic resistance to crack propagation, which corresponds to the fracture energy needed to initiate the propagation of the pre-crack when fibre bridging is absent. The total fracture energy, G_{IR}, is the driving force necessary to propagate the crack. Fig.3(a) shows the corresponding strain energy release plotted against the crack opening displacement. The bridging law can then be experimentally determined by optically measuring the crack opening displacement at the pre-crack tip location, δ_{a0}, together with the R-curve, and then by differentiating Eq. (6),

$$\delta_{sb}(\delta) = \frac{\partial G_{sb}}{\partial \delta_{a0}} \tag{7}$$

From the Eq. (7), the bridging law can then be obtained and the results are shown in Fig.3(b). It can be seen that the measured bridging law exhibit an exponential behaviour of large scale bridging reported in [24, 25, 33]. The static bridging stress distribution can be approximated by an exponential relationship,

$$\sigma_{sb}(x) = \sigma_{sb0} e^{-\gamma_s \delta(x)} \tag{8}$$

where σ_{sb0} and γ_s denote the maximum value and the rate of decay of the static bridging stress.

3.2. Delamination Fatigue

Fig. 4 shows the results of delamination growth rates plotted against the cyclic strain energy release rate ΔG_{eq} under mode I and II loading. Significant load ratio effects can be observed for mode I fatigue delamination behaviour, but not for mode II loading. The influence of load ratio under mode I, i.e. the higher the load ratio the faster the fatigue growth rates, is consistent with the fatigue behaviour of metals and bonded joints. This similarity indicates the presence of a certain mechanism affecting the crack tip conditions as in the case of metal and bonded joints where plasticity induced crack closure has been identified as the driving mechanism. It is also observed that the slope of the mode I delamination growth rate is almost twice than of mode II. Similar to the static case, fibre bridging was also postulated as the cause for the observed mode I behaviour.

In the constant strain energy release test, where $G_{\max}^{app}$ was kept constant, the delamination growth rate gradually decreases as the total delamination length increases, referring to Fig.5. At the early stage of crack growth from its initial position, the fatigue fibre bridging zone was not formed and no retardation of delamination growth was present. As the fatigue crack grew, an increasingly large fibre bridging zone was created behind the crack tip, leading to a decrease in crack propagation rates. After a crack propagation length of approximately 20 mm, the crack propagation rates were observed to attain a steady-state value, corresponding to the full development of the fibre bridging zone under fatigue.

3.3. Fibre Bridging Under Fatigue

A Scanning Electron Microscope (SEM) image of the side crack profile of a fatigue specimen shows the bridging by cross-over fibres in the crack wake, seen in Fig.6 (SEM image 1). A second SEM image was taken at a location further behind the crack tip. It is clear that bridging fibres are visible within the crack wake. The bridging fibres induce a traction stress across the crack faces, with the highest stress close to the crack tip and gradually decaying in a manner similar to the static case. Furthermore, the SEM images of the mode I fatigue samples presented in Fig. 7(a) show an uneven fracture plane. This suggests that there is no well-defined single crack propagation plane due to the nesting of the fibres that bridge the fatigue crack [31]. A large number of broken fibres can also be observed, evidencing fatigue degradation of the bridging zone. The morphology of the resin region, referring to Fig.7(b), shows a brittle fracture mechanism, indicating the absence of plastic deformation of the epoxy matrix. Unlike for metallic alloys and bonded joints, plasticity induced crack closure cannot be attributed for the observed load ratio effects in mode I fatigue behaviour of composite laminates. Consequently, this leaves fibre bridging as the only mechanistic explanation.

Under static loading, the fibre bridging traction relation can be determined using the J-integral method [23, 24, 33], as discussed in Section 3.1. However, the J-integral method is not applicable to characterising the fatigue bridging traction stress because (1) the precision of the optical measuring technique of small crack opening displacement lacks the necessary accuracy to enable numerical differentiation and (2) the applied sub-critical load amounts to a stationary crack under static conditions, hence it is impossible to obtain an equivalent R-curve. Murri [26] and Zhang et al. [32, 34] attempted to normalise the fatigue delamination resistance based from the static results, on the premise that the fatigue and static bridging relationships are identical. However Yao et al. [18] concluded that the bridging created in fatigue delamination is different from that pertinent to the static delamination at the same crack length. Stutz et al. [25] employed an inverse method to determine the tractions in the bridging zone in monotonic and fatigue loads and found that the under

small crack opening displacement (less than 0.5 mm) the bridging stress is higher under static loading than under fatigue loading, while at greater opening displacement the fatigue traction stress is higher than the static counterpart.

In the constant $G_{\max}^{app}$ fatigue test, the near-constant delamination growth rates were attained after a bridging zone length of 20 mm was formed. This suggests beyond this delamination growth increment the fatigue bridging zone developed fully and the opening crack profile became self-similar (independent of delamination length). In the next section we present an inverse solution method to determine the fatigue fibre bridging parameters.

4. Inverse solution of fibre bridging law

4.1. Method

Unlike the static fracture where the fibre bridging stress can be determined from the R-curve measured under rising load, a different method is required to determine the traction stress, referring to Fig.8(a), under steady-state fatigue delamination crack growth. The bridging law is approximated as an exponential function, shown in Fig.8(b), and is defined as follows,

$$\sigma_{fb}(x) = \sigma_{fb0} e^{-\gamma_f \delta(x)} \tag{9}$$

where γ_f accounts for the rate of decay of the traction stress from the crack tip ($\gamma_f > 0$), and σ_{fb0} denotes the maximum bridging traction stress at the tip of a steady-state fatigue crack. In the following an inverse method is presented, involving two steps. Firstly, the crack opening displacements at different positions behind the tip of steady-state fatigue crack were experimentally measured. The results for $G_{\max}^{app}$=150 J/m^2 are shown in Fig.8(c). Denoting this opening displacement as $\delta_f(x)$, where the subscript *f* denotes the opening displacement pertinent to fatigue, and *x* the distance behind the crack tip, when the specimen is subjected to the maximum applied displacement used for the fatigue test. In the second step, the fatigue bridging parameters are determined from an inverse solution method. To achieve this, the fibre bridging process is represented by a surface traction stress distribution, acting in the y-direction. To find the appropriate values of γ_f and σ_{fb0}, a finite element model of the DCB specimens is developed with the fibre bridging being represented by the traction stress given by Eq.(9) acting in the direction perpendicular to the crack face over a distance of 25 mm. Due to symmetry in the present case, it is sufficient to model half of the DCB specimen. The appropriate values of γ_f and σ_{fb0} are to be determined by minimising the difference between the crack opening displacements measured experimentally and computed from the FE analysis, i.e. minimising the following cost function,

$$F\left(\gamma_f, \sigma_{fb0}\right) = \int_0^{\Delta a_{fb}} \left[\frac{\delta_{FEM}(x) - \delta_{EXP}(x)}{\delta_{EXP}\left(\Delta a_{fb}\right)} \right]^2 dx \qquad (10)$$

where $\delta_{EXP}(x)$ and $\delta_{FEM}(x)$ are the crack opening displacements measured experimentally and computed by the FE model, respectively. The parameter Δa_{fb} denotes the fibre bridging zone length. The above cost function serves as the objective function to reduce the error between numerical and experimental values during the optimisation process.

FE analyses were performed using commercial software Abaqus Standard v6.11. The substrate of the DCB was modelled using four-noded reduced integration plane strain (CPE4R) elements. Reduced integration elements were used to avoid shear locking of the elements under large bending deformations. The properties of the composite laminate are E_{11} = 131 GPa, $E_{22} = E_{33}$ = 13 GPa, $G_{13} = G_{23}$ = 6.4 GPa, $\nu_{12} = \nu_{13} = \nu_{23}$ = 0.35. In the present work, a genetic algorithm available in commercial software ModeFrontier [35] is employed to search the appropriate values of γ_f and σ_{fb0} that will minimise the cost function of Equation (10). To ensure convergence to the optimum solution, the genetic algorithm employs an elitism method. Essentially the best individual in the current population is kept as the best solution in the next iteration if no better solution is found in the next iteration; otherwise the new best solution is taken as the new best overall solution. In this way, the fitness value of the best individual defines an increasing and upper bounded sequence, so it converges to the optimal solution.

The values of the cost function during 300 iterations are plotted in Fig.8(d). It can be seen that the optimisation solution achieved a minimum solution after about 120 iterations; more iterations did not yield any further improvement. This inverse method is highly robust, with rapid convergence independent of the initial values of γ_f and σ_{fb0}. The fatigue bridging law corresponding to the best solution according to this inverse method is presented in Fig.9. The values of the fatigue bridging stress (σ_{fb0}) and the rate of decay (γ_f) are equal to 0.225 MPa and 3.21, respectively.

4.2. Validation of the inverse method

To validate the inverse method for determining the fatigue fibre bridging relationship, the inverse method is applied to obtain the static bridging traction law from the crack opening displacement data presented in Fig.8(c). As in the fatigue case, the appropriate values of σ_{sb0} and γ_s are taken as those minimising the cost function of Equation (10), substituting Δa_{fb} and $\delta_{EXP}(x)$ with the static results

presented in Fig.8(c). The finite element results $\delta_{FEM}(x)$ are computed using Equation (10), with experimentally determined values of σ_{sb0} and γ_s as the initial guess. It is clear that the inverse method gives a very similar solution as the J-integral method, further substantiating the inverse method. This result confirms the validity of the inverse method. It is very interesting to note that the maximum fatigue traction stress σ_{fb0} determined by the inverse method presented in Section 4.1 is approximately equal to the maximum static traction stress for the static bridging zone, i.e. $\sigma_{fb0} \approx \sigma_{sb0}$, providing further support to the inverse method.

A comparison of the bridging relationships developed under static and fatigue loads is shown in Fig.9. The maximum traction stress of the fatigue bridging law is very similar to the static bridging law, but the fatigue bridging law exhibits a much faster decay with opening displacement than under static fracture. This is likely due to the cyclic degradation of the bridging fibres due to fatigue loading. To simulate the crack propagation under static loads as shown in Fig. 10(a), it is important to incorporate the two fracture processes pertinent to the matrix (i.e. creation of new crack surfaces) and fibre bridging under static loading into the traction-separation laws, presented in Fig.10(b). Specifically, the static bridging law is the combination of the two separate traction laws operating over two different length scales. To illustrate the importance of accounting for the fibre bridging process, three different traction laws were used in a FE analysis of the crack propagation under static loads. The traction laws are denoted as A, B and C; their details are listed in Table 1. The load-displacement responses from numerical simulations and experiments are shown in Fig. 10(c). Ignoring the contribution from fibre bridging, traction law A can only predict the onset of non-linearity. Similarly, traction law B, which accounts for the total energy contribution from the matrix and fibre bridging using a linear degradation (identical fracture energy as but small scale bridging) relationship, fails to accurately predict the experimental data. It is clear that only when the behaviour of large scale bridging is modelled by traction law C can the experimental load-displacement response be accurately predicted. Shown in Fig.10(d) are the results of the R-curve of the DCB specimen. Here G_{IRC} of the finite element analysis result was determined from the load-displacement response using Eq. (4). Hence the bridging parameters approximated by the exponential traction law in the inverse solution method are validated by the experimental measurements and finite element simulations.

5. Crack-tip shielding by fibre bridging under fatigue

Fibre bridging reduces the crack growth driving force at the tip of a fatigue delamination crack to below the applied strain energy release rate. To quantify this reduction, a cohesive zone model, schematically shown in Fig.11(a) was used to investigate the crack shielding effect on a fatigue crack under subcritical loads as a result of fibre bridging. Under steady-state crack growth condition, the fatigue fibre-bridging zone is fully developed. This bridging zone can be represented by cohesive elements, referring to Fig. 11(b), with the traction law D shown in Fig.9 and listed in Table 1. The length of cohesive zone was set at 40 mm to ensure the fibre-bridging zone to be fully developed (the steady-state bridging zone length is approximately 30 mm). The parameter G^{tip} represents the actual strain energy release rate experienced at the crack tip and was determined using the virtual crack closure technique [36]. G^{app} is the strain energy release rate calculated based on the global response of the DCB with beam theory. During the loading portion of the cycle, the cohesive elements in the wake of the crack gradually open up. When the applied load is below a certain level, such as that the applied strain energy release rate G^{app} remains less than fatigue fibre bridging energy G_{fb}, the crack-tip remains closed with the effective strain energy release rate being zero, as shown in Fig.11(d). Only when the applied strain energy release rate G^{app} exceeds the fatigue fibre bridging energy does the crack tip experiences positive driving force. The results of the crack tip strain energy release rate presented in Fig.11(d) are well approximated by the following relationship,

$$G_{\max}^{tip} = \begin{cases} 0 & G_{\max}^{app} < G_{fb} \\ G_{\max}^{app} - G_{fb} & G_{\max}^{app} \geq G_{fb} \end{cases} \tag{11}$$

which is consistent with the J-integral solution. For the present composite material system, G_{fb} has been calculated using the cohesive model, i.e. $G_{fb} = \sigma_{fb0} / \gamma_f = 70 \text{ J/m}^2$.

During the unloading phase of a fatigue cycle, all the cohesive elements un-load elastically, referring to Fig. 11(c), and experience no further fatigue damage. The crack-tip strain energy release rate returns proportionally to the origin, as shown in Fig.11(d). As a result, the minimum value of the crack-tip strain energy release rate is,

$$G_{\min}^{tip} = \begin{cases} R^2 G_{\max}^{tip} & R \geq 0 \\ 0 & R < 0 \end{cases} \tag{12}$$

It can readily shown that without fibre bridging, it can be seen that G^{tip} is equal to G^{app}.

6. A New Scaling Parameter For Fatigue Delamination Growth

Having quantified the parameters of the fatigue bridging law and the effects of bridging on the crack tip, a new scaling parameter can now be defined to describe the delamination tip conditions for fatigue. By isolating the influence of fibre bridging, the crack tip conditions represent the intrinsic toughness of the matrix to fatigue crack growth (although not necessarily the neat polymer property). Hence ΔG^{tip} is used to correlate with the fatigue crack growth. The proposed scaling parameter is defined as the effective cyclic strain energy release rate given below,

$$\Delta G_{eff} = \Delta G^{tip} = (\sqrt{G^{tip}_{\max}} - \sqrt{G^{tip}_{\min}})^2 \tag{13}$$

After inserting Equations (11) and (12), the effective cyclic strain energy release rate can be written as

$$\Delta G_{eff} = \begin{cases} (G^{app}_{\max} - G_{fb})(1-R)^2 & R \geq 0 \\ G^{app}_{\max} - G_{fb} & R < 0 \end{cases} \tag{14}$$

It is clear that this new parameter reduces to the equivalent strain energy release rate given by Equation (3) when the fibre bridging effect is ignored.

As already noted in Fig.4, at high strain energy release rates, the proximity of the maximum strain energy release rate to the critical fracture energy strongly influences delamination growth. To account for this effect, the Forman model can be adapted to remove the influence of $G^{app}_{\max}$. The delamination growth rate can now be expressed in terms of the effective strain energy release ΔG_{eff} and the critical strain energy release rate G_c,

$$\frac{da}{dN} = \frac{C_F \left(\Delta G_{eff}\right)^{m_F}}{(1-R)\left(\sqrt{G^{tip}_{IRC}} - \sqrt{G^{tip}_{\max}}\right)} = \frac{C_F \left(\Delta G_{eff}\right)^{m_F}}{(1-R)\left(\sqrt{G_{IRC} - G_{fb}} - \sqrt{G^{app}_{\max} - G_{fb}}\right)} \tag{15}$$

where $G^{tip}_{IRC} = G_{IRC} - G_{fb}$ and $G^{tip}_{\max} = G^{app}_{\max} - G_{fb}$ have been used. The parameter G_{IRC} is the steady state fracture toughness obtained from the static R-curve tests.

At each experimental data point, the Forman model represents the data by computing the factored rate of delamination growth.

$$Q_{br} = (1-R)\left(\sqrt{G_{IRC} - G_{fb}} - \sqrt{G^{app}_{\max} - G_{fb}}\right)\frac{da}{dN} = C_F \left(\Delta G_{eff}\right)^{m_F} \tag{16}$$

The correlations between experimental data of different load ratios using the new scaling parameter in conjunction with the Forman model are shown in Fig. 12(a). A unique solution of C_F and m_F can be obtained which is determined to be 2.5×10^{-15} and 5.32 respectively. It can also be observed that

the slope of the Forman plot ($m_F = 5.32$) is now significantly lower than that obtained without accounting for fibre bridging (m = 10 for R = 0.1, m = 12.8 for R = 0.3 and m = 15.7 for R = 0.5, as shown in Fig.4). Fig. 12(b) compares the experimentally measured delamination growth rates against the effective strain energy release rates predicted by using the derived Forman parameters. It can be seen that Eq. (15) is able to correlate to the experimental delamination growth data in the Paris plot.

The load shedding method typically used for determining the delamination growth rates poses two challenges for composite laminates. Firstly, the initial bridging zone is small and therefore the crack growth rate will be high. As the bridging zone develops, the delamination growth rates retards and this leads to an artificially high slope in the Paris law relation. Using the proposed scaling parameter in Eq. (14), the crack shielding effect due to a fully developed bridging zone can be accounted for where G_{fb} can be determined by the inverse solution method, described in Section 4. The modified Forman model enables the transient effect of a developing bridging zone on fatigue delamination growth rate to be taken into account. Consequently, the true threshold value can be selected as a design parameter. Assuming that threshold for very slow delamination growth taken at 10^{-8} m/cycle [29], the mode I and II threshold value can be taken at 27.5 J/m^2 and 200 J/m^2 respectively which represents 27% and 20% of the delamination onset value under static loads.

7. Conclusions

Significant load ratio effects were observed experimentally in the fatigue delamination growth of composite laminates. No existing correlating parameter is capable of mechanistically explaining these effects, as traditional approaches have relied predominately on empirical curve fitting. Experimental investigations confirmed the strong influence of mean loads in the mode I fatigue behaviour when correlated with the equivalent strain energy release rate. As in the case of metallic alloys and bonded joints, this phenomenon signifies non-linear conditions at the crack tip, arising from fibre bridging in the crack wake. An inverse method has been developed to quantify the fibre bridging law under static and fatigue loading. By accounting for the effect of fibre bridging, a new scaling parameter has been proposed to quantify the effects of mean load on mode I fatigue delamination growth rates. The new correlating parameter, which conforms to the similitude requirement, is able to unify the mode I fatigue delamination growth rates under different load ratios.

Acknowledgements

This work was undertaken within the Robust Composite Repair project, part of a CRC-ACS research program, established and supported under the Australian Government's Cooperative Research Centres Program.

Reference

[1] FAA. Composite Aircraft Structure: Advisory Circular (AC) 20-107B, Change 1. FAA; 2010.

[2] Goh JY, Georgiadis S, Orifici AC, Wang CH. Effect of disbonds on the fatigue endurance of composite scarf joints. Advanced Materials Research. 2014;891-892:191-196.

[3] Wang CH. Fracture of interface cracks under combined loading. Engineering Fracture Mechanics. 1997;56(1):77-86.

[4] Schön J. A model of fatigue delamination in composites. Composites Science and Technology. 2000;60(4):553-558.

[5] Erpolat S, Ashcroft IA, Crocombe AD, Abdel-Wahab MM. Fatigue crack growth acceleration due to intermittent overstressing in adhesively bonded CFRP joints. Composites Part A: Applied Science and Manufacturing. 2004;35(10):1175-1183.

[6] Hojo M, Ochiai S, Gustafson C-G, Tanaka K. Effect of matrix resin on delamination fatigue crack growth in CFRP laminates. Engineering Fracture Mechanics. 1994;49(1):35-47.

[7] Hojo M, Tanaka K, Gustafson CG, Hayashi R. Effect of stress ratio on near-threshold propagation of delimination fatigue cracks in unidirectional CFRP. Composites Science and Technology. 1987;29(4):273-292.

[8] Matsubara G, Ono H, Tanaka K. Mode II fatigue crack growth from delamination in unidirectional tape and satin-woven fabric laminates of high strength GFRP. International Journal of Fatigue. 2006;28(10):1177-1186.

[9] Rans C, Alderliesten R, Benedictus R. Misinterpreting the results: How similitude can improve our understanding of fatigue delamination growth. Composites Science and Technology. 2011;71(2):230-238.

[10] Donough MJ, Gunnion AJ, Orifici AC, Wang CH. Plasticity induced crack closure in adhesively bonded joints under fatigue loading. International Journal of Fatigue. 2015;70:440-450.

[11] Donough MJ. Load ratio effect in the fatigue crack propagation of composite laminates and bonded joints PhD Thesis. RMIT University, Aerospace, Mechanical and Manufacturing Engineering, 2014.

[12] Andersons J, Hojo M, Ochiai S. Empirical model for stress ratio effect on fatigue delamination growth rate in composite laminates. International Journal of Fatigue. 2004;26(6):597-604.

[13] Allegri G, Jones MI, Wisnom MR, Hallett SR. A new semi-empirical model for stress ratio effect on mode II fatigue delamination growth. Composites Part A: Applied Science and Manufacturing. 2011;42(7):733-740.

[14] Allegri G, Wisnom MR, Hallett SR. A new semi-empirical law for variable stress-ratio and mixed-mode fatigue delamination growth. Composites Part A: Applied Science and Manufacturing. 2013;48(0):192-200.

[15] Jones R, Pitt S, Bunner AJ, Hui D. Application of the Hartman–Schijve equation to represent mode I and mode II fatigue delamination growth in composites. Composite Structures. 2012;94(4):1343-1351.

[16] Jones R, Hu W, Kinloch AJ. A convenient way to represent fatigue crack growth in structural adhesives. Fatigue & Fracture of Engineering Materials & Structures. 2014:n/a-n/a.

[17] Khan R, Rans C, Benedictus R. Effect of stress ratio on delamination growth behaviour in unidirectional carbon/epoxy under mode I fatigue loading. ICCM, Edinburgh, UK2009.

[18] Yao L, Alderliesten R, Zhao M, Benedictus R. Bridging effect on mode I fatigue delamination behavior in composite laminates. Composites Part A: Applied Science and Manufacturing. 2014;63(0):103-109.

[19] Anderson TL. Fracture Mechanics-Fundamentals and Applications. Boca Raton, Florida: CRC Press; 1995.

[20] Newman JCJ. FASTRAN-II: a fatigue crack growth structural analysis program. NASA Technical Memorandum 104159,Langley Research Centre, Hampton, Virginia, USA; 1982.

[21] Rose LRF, Wang CH. Self-similar analysis of plasticity-induced closure of small fatigue cracks. Journal of the Mechanics and Physics of Solids. 2001;49(2):401-429.

[22] Wang CH, Rose LRF, Newman JC. Closure of plane-strain cracks under large-scale yielding conditions. Fatigue & Fracture of Engineering Materials & Structures. 2002;25(2):127-139.

[23] Sørensen BF, Jacobsen TK. Large-scale bridging in composites: R-curves and bridging laws. Composites Part A: Applied Science and Manufacturing. 1998;29(11):1443-1451.

[24] Sorensen L, Botsis J, Gmür T, Humbert L. Bridging tractions in mode I delamination: Measurements and simulations. Composites Science and Technology. 2008;68(12):2350-2358.

[25] Stutz S, Cugnoni J, Botsis J. Studies of mode I delamination in monotonic and fatigue loading using FBG wavelength multiplexing and numerical analysis. Composites Science and Technology. 2011;71(4):443-449.

[26] Murri GB. Effect of data reduction and fiber-bridging on Mode I delamination characterization of unidirectional composites. Journal of Composite Materials. 2014;48(19):2413-2424.

[27] ASTM. D5528. Standard test method for mode I interlaminar fracture toughness of unidirectional fiber-reinforced polymer matrix composites, West Conshohocken, PA: ASTM International; 2001(2013).

[28] DIN. EN 6034. Aerospace Series - Carbon fibre reinforced plastics - Test method - Determination of interlaminar fracture toughness energy Mode II - GIIC, 1995.

[29] Al-Khudairi O, Hadavinia H, Waggott A, Lewis E, Little C. Characterising mode I/mode II fatigue delamination growth in unidirectional fibre reinforced polymer laminates. Materials & Design. 2015;66, Part A:93-102.

[30] ASTM. E647. Standard test method for measurement of fatigue crack growth rates, West Conshohocken, PA: ASTM International; 2013.

[31] Johnson WS, Mangalgiri PD. Investigation of fiber bridging in double cantilever beam specimens. NASA; 1986. p. 22.

[32] Zhang J, Peng L, Zhao L, Fei B. Fatigue delamination growth rates and thresholds of composite laminates under mixed mode loading. International Journal of Fatigue. 2012;40(0):7-15.

[33] Suo Z, Bao G, Fan B. Delamination R-curve phenomena due to damage. Journal of the Mechanics and Physics of Solids. 1992;40(1):1-16.

[34] Peng L, Zhang J, Zhao L, Bao R, Yang H, Fei B. Mode I delamination growth of multidirectional composite laminates under fatigue loading. Journal of Composite Materials. 2011;45(10):1077-1090.

[35] ModeFrontier User Manual Version 4.5. Trieste, Italy: ESTECO s.p.a; 2014.

[36] Krueger R. The virtual crack closure technique: History, approach and applications. Hampton, VA: NASA; 2002. p. 64.

Tables

Table 1: Input parameters of cohesive law used in numerical simulations

Traction law	Traction law description	k^0 (N/mm^3)	σ^0 (MPa)	G_{IC0} (kJ/m^2)	k_{br} (N/mm^3)	σ_{br0} (MPa)	δ_f (mm)
A	Without fibre bridging (matrix toughness only)	1E6	40	0.1	-	-	-
B	Lumped fibre bridging and matrix toughness	1E6	40	0.24	-	-	-
C	Fibre bridging and matrix cohesive zone	1E6	40	0.1	-	0.236	1.42
D	Fatigue fibre bridging only				240	0.225	3.21

Figures

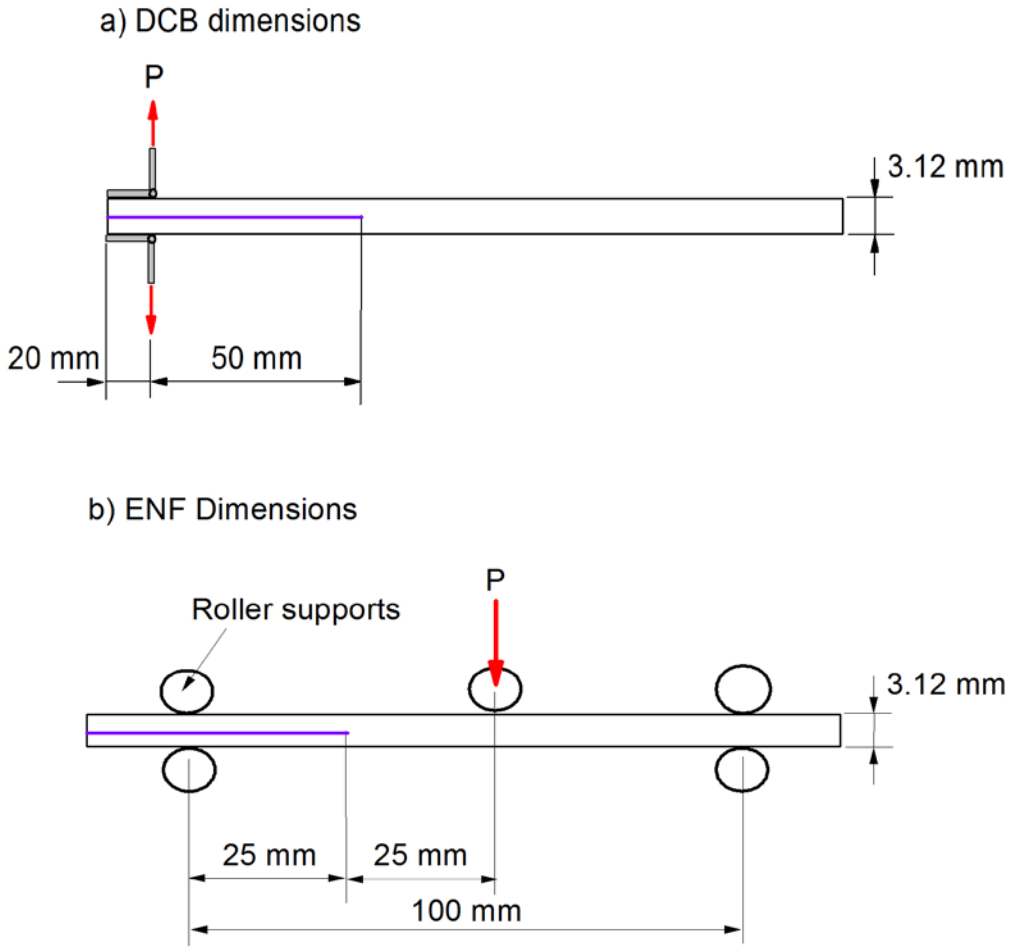

Fig. 1. Schematic of DCB and ENF test configurations

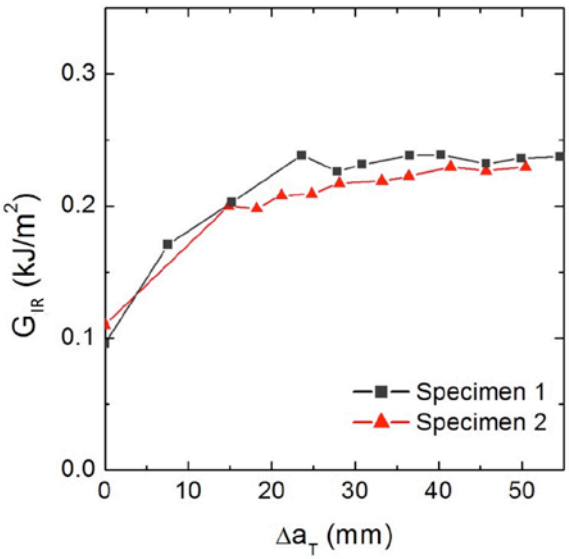

Fig. 2. Mode I strain energy release rate versus crack growth increment from static DCB tests.

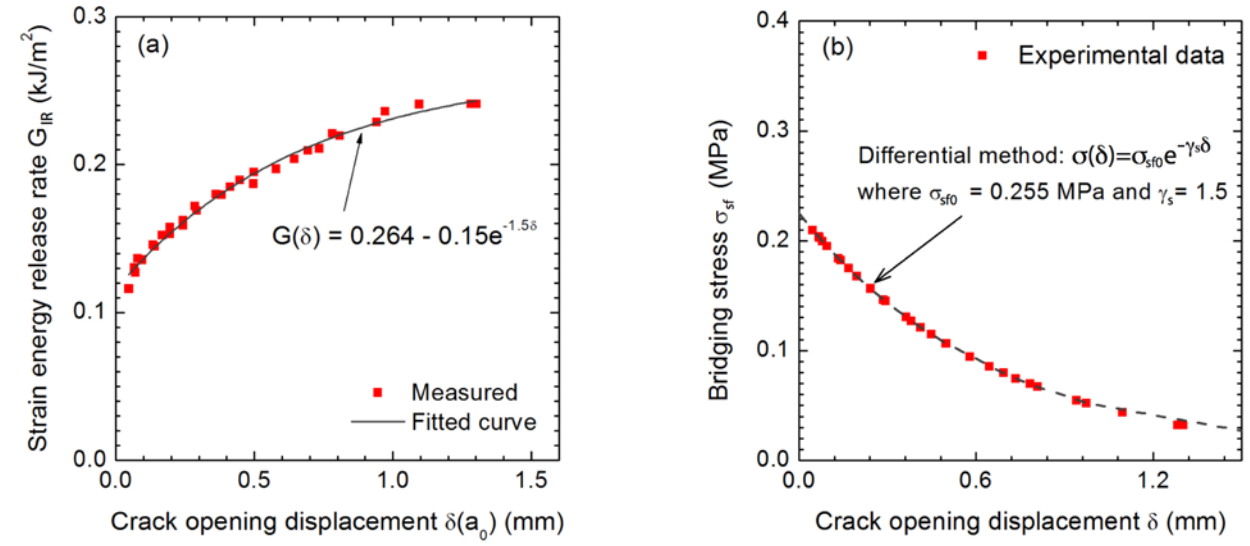

Fig. 3. (a) Measured G_{IR} versus crack opening displacement and (b) calculated bridging traction stress versus crack opening displacement under static loading.

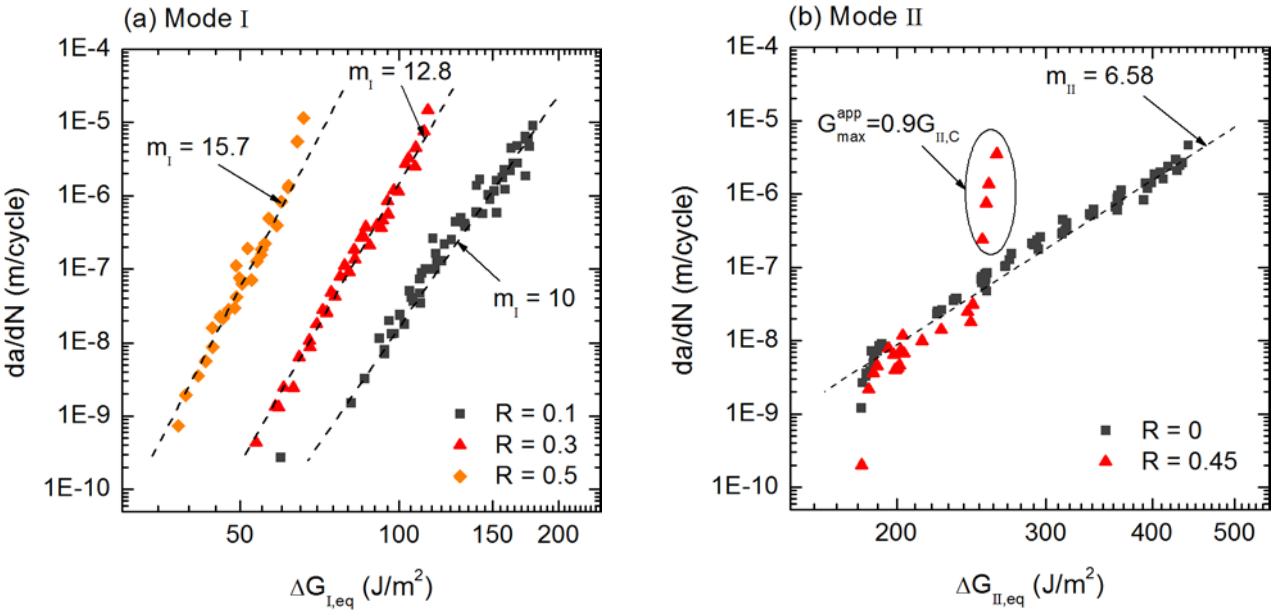

Fig. 4. Relation between fatigue delamination growth rates and cyclic strain energy release rate ΔG_{eq} under (a) mode I and (b) mode II loading

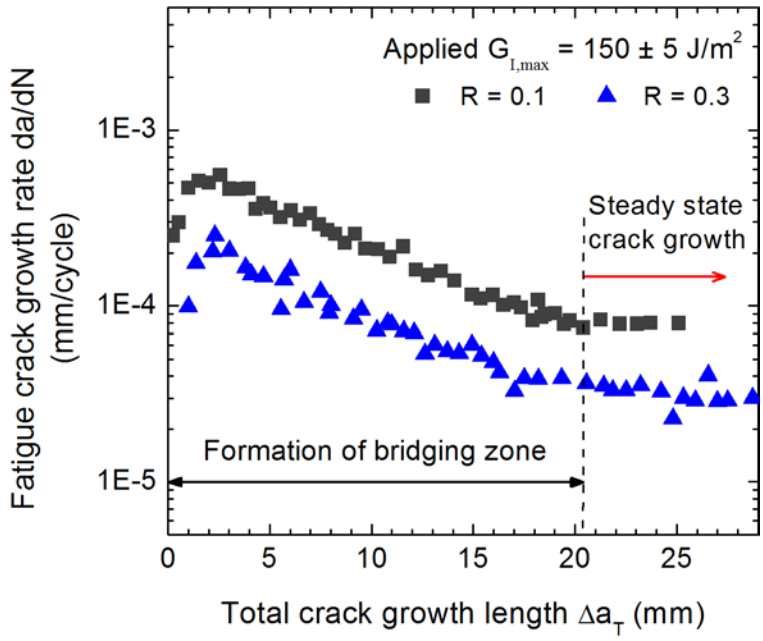

Fig. 5. Fatigue delamination growth rates versus the growth length in a constant G_{max} test

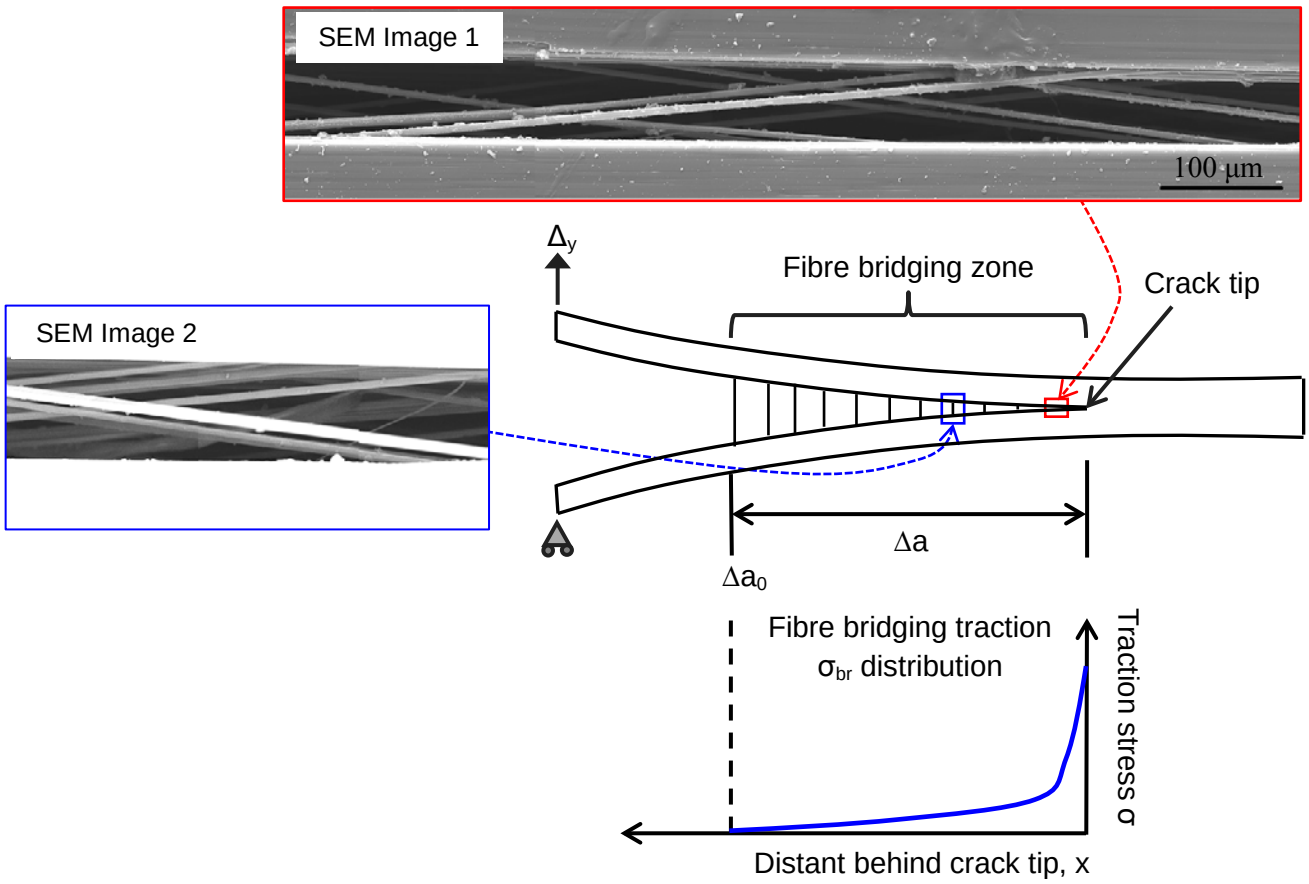

Fig. 6. Schematic of crack bridging by cross-over fibres in the wake of delamination after the crack has propagated for a distance of Δa

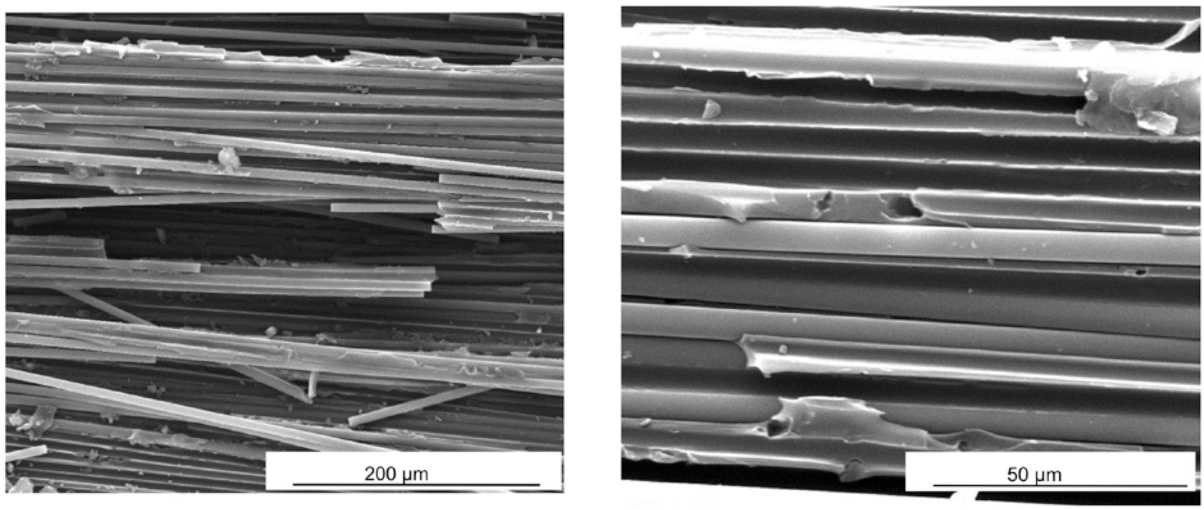

Fig. 7. SEM images of the fracture surfaces under mode I fatigue loading exhibiting (a) broken fibres and (b) residual matrix

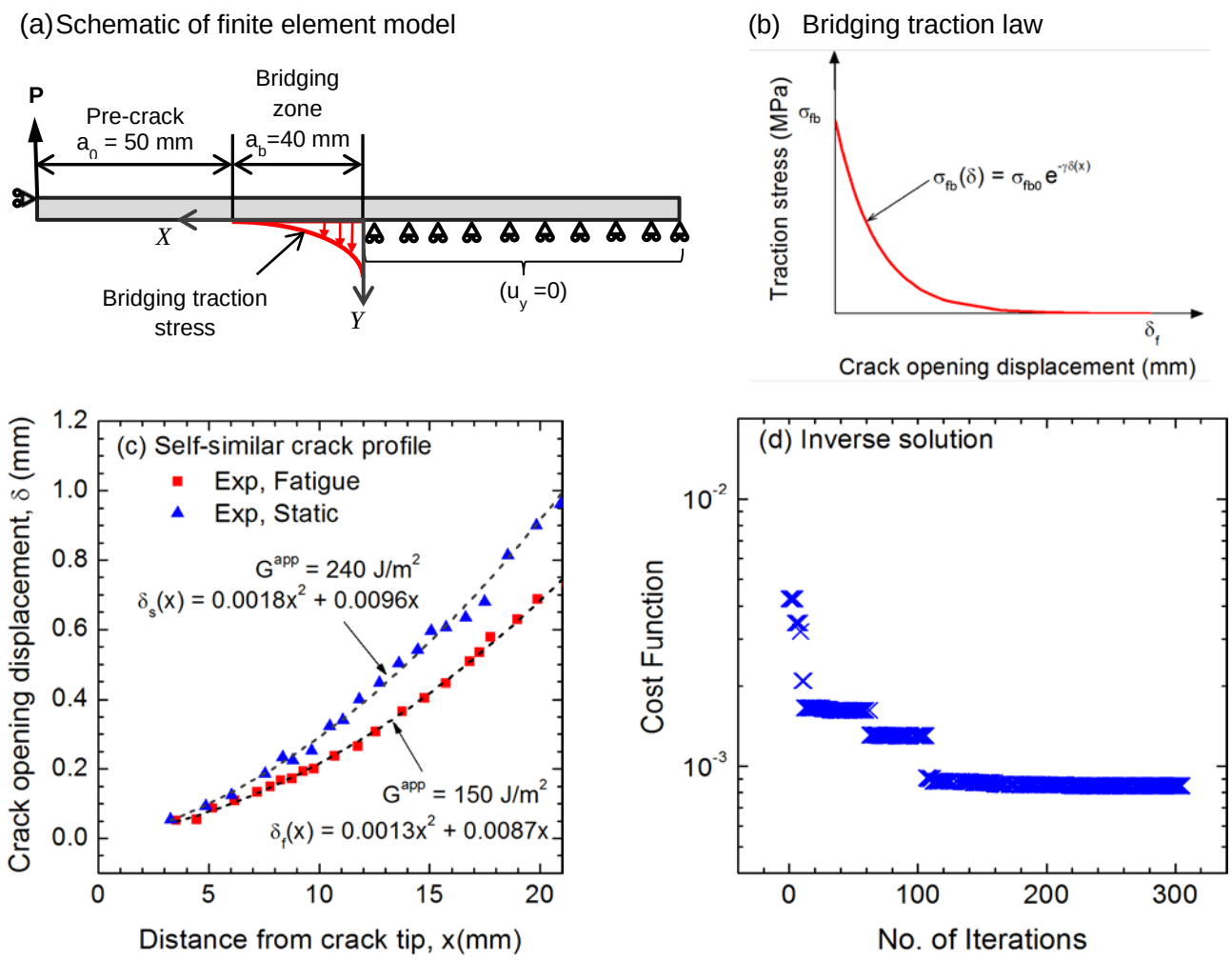

Fig. 8. (a) Schematic of finite element model used, (b) fibre bridging traction law, (c) the opening profile behind the tip of a fatigue delaminate crack and (d) values of the cost function versus the number of optimisation iterations.

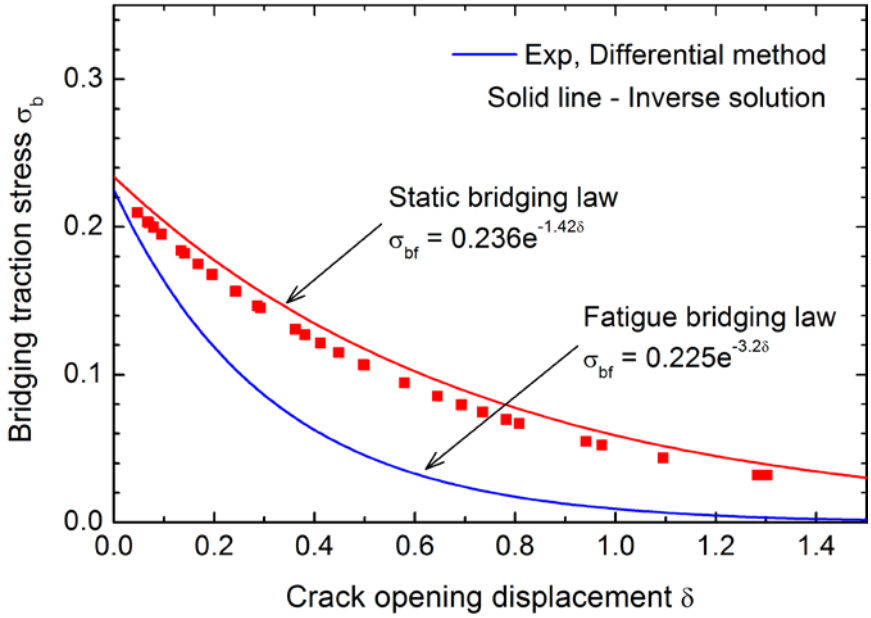

Fig. 9. Comparison for fibre bridging stresses under static and steady state fatigue loading

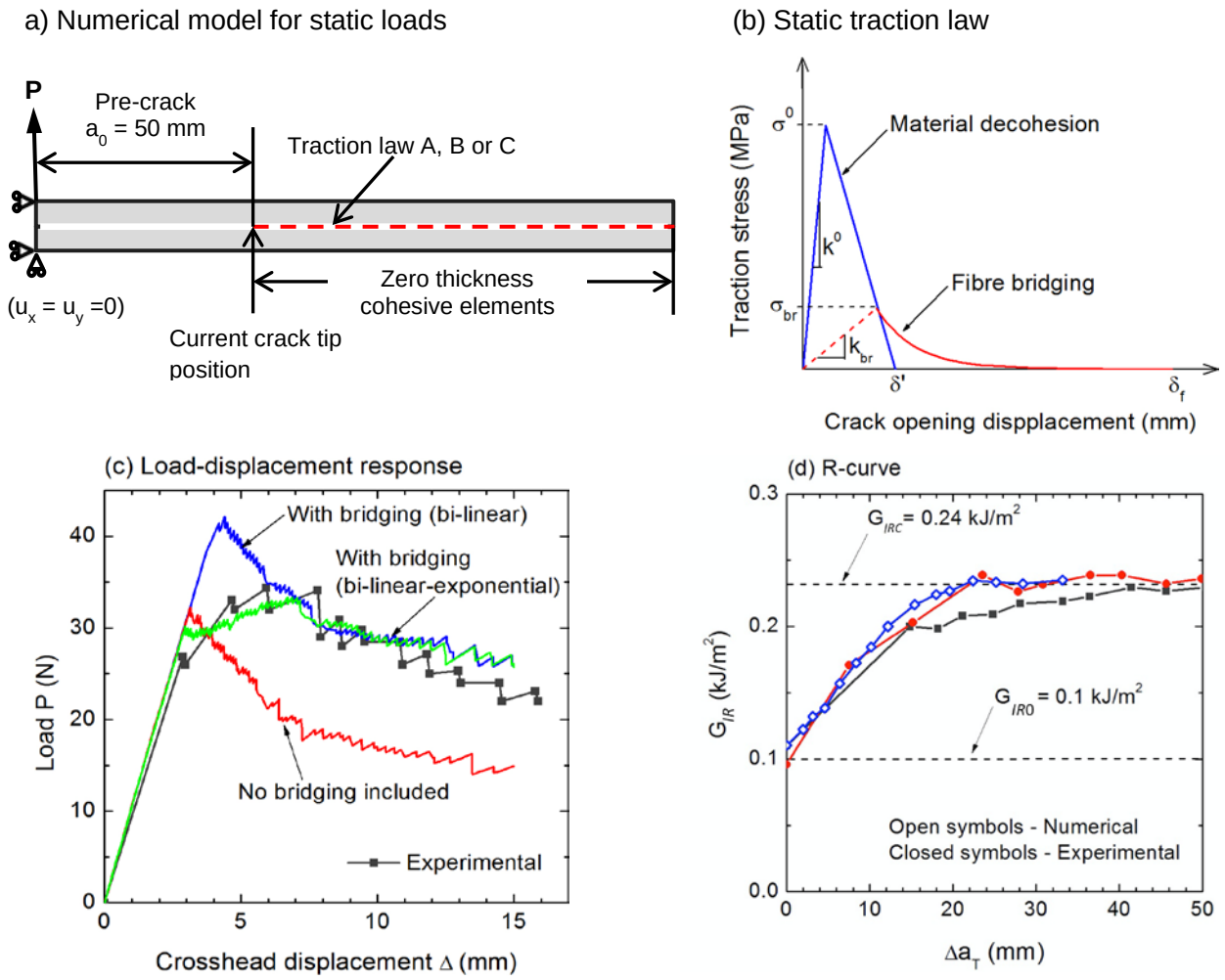

Fig. 10. (a) Schematic of finite element model used, (b) static traction law description and comparison of the experimental and finite element analysis results for (c) static load-displacement responses and (d) the *R*-curve mode I delamination cracking

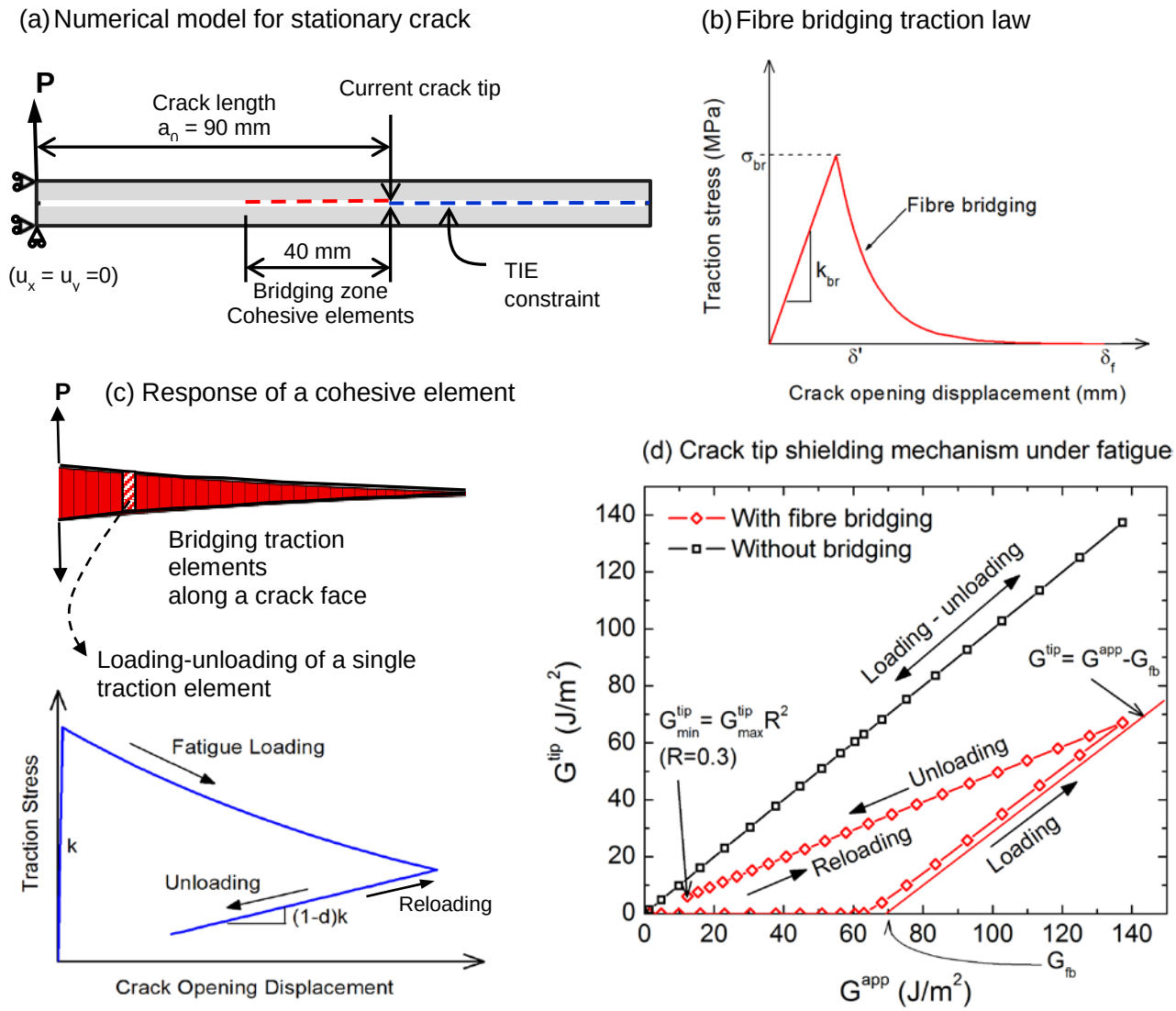

Fig. 11. (a) Schematic of finite element model used, (b) traction law incorporating only the large scale fibre bridging component, (c) the loading-unloading process of a traction element and (d) Crack tip shielding mechanism as a result of fibre bridging

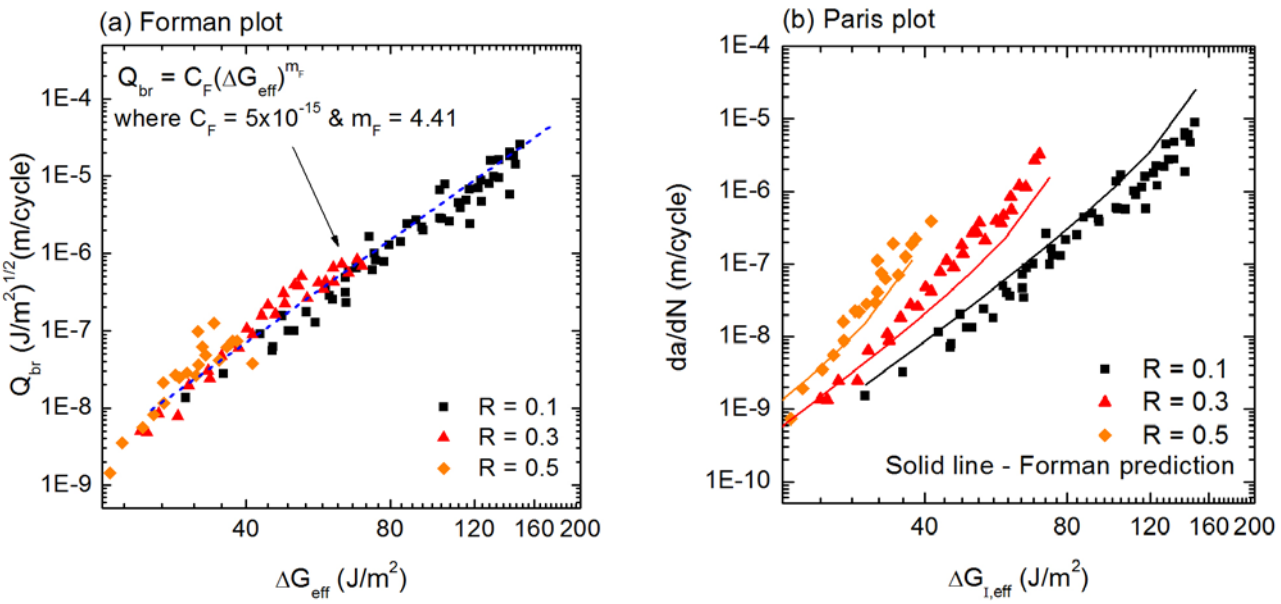

Fig. 12. Mode I experimental data under varying load ratios correlated with ΔG_{eff} by accounting for fibre bridging; (a) Forman plot and (b) Paris plot